Supporting Information

Activation of Persulfate by Nanosized Zero-valent Iron (NZVI): Mechanisms and Transformation Products of NZVI

Cheolyong Kim[1], Jun-Young Ahn[1], Tae Yoo Kim[1], Won Sik Shin[2], and Inseong Hwang[1*]

[1]Department of Civil and Environmental Engineering, Pusan National University, Busan 46241, Republic of Korea

[2]School of Architecture, Civil, Environmental and Energy Engineering, Kyungpook National University, Daegu 41566, Republic of Korea

* Corresponding author:

Inseong Hwang, Department of Civil and Environmental Engineering, Pusan National University, 2, Busandaehak-ro 63beon-gil, Geumjeong-gu, Busan 46241, Republic of Korea

E-mail address: ihwang@pusan.ac.kr; phone: +82-51-510-3523; fax: +82-51-514-9574

Contents: 21 pages, 2 texts, 4 tables, 13 figures and a scheme.

Texts

Tables

Figures

Scheme

Changes in pH of buffered solutions treated with persulfate/NZVI process

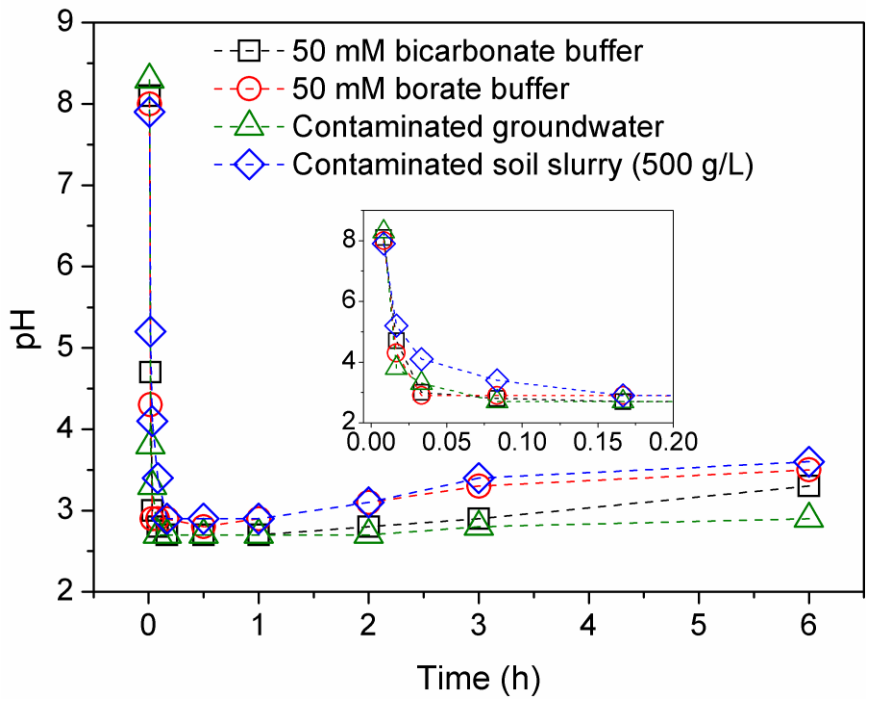

Figure S1. Changes in pH of (a) borate (50 mM) buffered solution, (b) bicarbonate (50 mM) buffered solution, (c) contaminated groundwater, and (d) contaminated soil slurry (500 g/L) treated with persulfate/NZVI process

Measurements and analyses

Text S1. Instrumentation and chemicals used

Phenol and its aromatic intermediates. Phenol, catechol, hydroquinone, and 1,4-benzoquinone were quantified using a high-performance liquid chromatograph equipped with a UV detector (SPD-20A; Shimadzu, Japan) and a C18 column (Poroshell 120; Agilent Technologies, USA). The mobile phase was 20% acetonitrile (99.8% pure; J.T. Baker) in water. Phenol and catechol

were detected using a wavelength of 275 nm, and 1,4-benzoquinone and hydroquinone using wavelengths of 250 and 300 nm, respectively.

Persulfate. The persulfate concentration was determined using a method published by Fang et al.[1] but using a smaller sample volume. A chromogenic reagent containing 1000 g/L potassium iodide (99.5% pure; Junsei Chemical Co.) and 5 g/L sodium bicarbonate (99.5% pure; Junsei Chemical Co.) was prepared. The reagent was allowed to equilibrate for 15 min, then 10 mL was transferred into a 15 mL polypropylene centrifuge tube. A 0.25 mL aliquot of a sample from a batch test was added to the tube, then the mixture was mixed thoroughly for a few seconds and then allowed to stand for 20 min. The solution was yellow, and absorbance was measured at 400 nm using a Optizen Pop UV-Vis spectrometer (Mecasys, Korea).

Dissolved iron. The dissolved iron concentration was measured using the 1,10-phenanthroline method. A 0.5 mL aliquot of a filtered sample was added to a centrifuge tube containing 5 mL of a 1.0% sodium citrate (99% pure; Junsei Chemical Co.) solution to allow the Fe^{2+} concentration to be determined. Another 0.5 mL aliquot of the filtered sample was added to a tube containing 5 mL of a 1.0% sodium citrate and 1.0% hydroxylamine hydrochloride (99% pure; Sigma-Aldrich) solution to allow the total dissolved Fe concentration to be determined. Then, 0.1 mL of 10% 1,10-phenanthroline (reagent grade; Sigma-Aldrich) in ethanol was added to each tube, and the tubes were allowed to stand for 20 min. Absorbance at 510 nm was measured using a UV-Vis spectrometer.

XRD. XRD analysis was performed using an XRD 6000 instrument (Shimadzu) using Cu Kα radiation ($\lambda = 1.5406$). A continuous scan from 5° to 80° was performed using a step size of 0.017°. The X-ray diffractogram was interpreted using PDF2 search software (X'Pert Highscore Plus; PANalytical, Netherlands).

SEM-EDS. Solid NZVI samples were placed onto a mount and then sputter-coated with Pt. The samples were analyzed using a SUPRA40VP SEM instrument (Zeiss, Germany) equipped with an Apollo EDS system (Edax, USA). The EDS was operated at 15 keV and using a setting of 50 live seconds.

X-ray absorption spectroscopy. X-ray absorption spectroscopy was performed at the Pohang Accelerator Laboratory (Korea) using the 8C beamline equipped with a Si(111) double crystal monochromator. Energy and current of electron storage ring were 3.0 GeV and ~300 mA, respectively. Fe K-edge (7112 eV) X-ray absorption spectra including X-ray absorption near edge structure and EXAFS spectra were collected at room temperature in transmission mode. The spectra were interpreted using IFEFFIT version 1.2.11 software. The spectra were energy-normalized and calibrated. Linear combination fitting was performed using the EXAFS spectra of standard Fe minerals (ferrihydrite, lepidocrocite, maghemite, magnetite, melanterite, metallic Fe, pyrite, schwertmannite, and wüstite).

TEM. TEM images were obtained at Korea Basic Science Institute Busan Center, using a JEM2100F 200 kV field-emission electron transmission microscope (Zeol, Japan).

Reactions involved with persulfate activation by NZVI

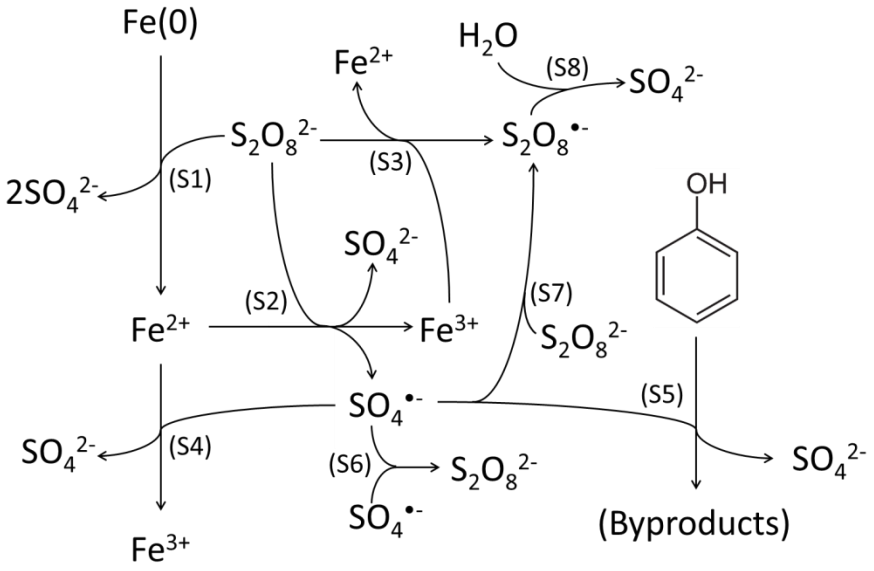

Scheme S1. Pathways involved in the activation of persulfate by Fe species

Text S2. Persulfate activation by NZVI and the fate of the sulfate radicals

Persulfate can be decomposed by $Fe^0_{(s)}$, $Fe^{2+}_{(aq)}$, and $Fe^{3+}_{(aq)}$. Persulfate oxidizes $Fe^0_{(s)}$ to form $Fe^{2+}_{(aq)}$ (reaction S1). Persulfate is transformed into the sulfate radical ($SO_4^{\bullet-}$) and the persulfate radical ($S_2O_8^{\bullet-}$) when it reacts with $Fe^{2+}_{(aq)}$ and $Fe^{3+}_{(aq)}$, respectively (reactions S2 and S3).

$$S_2O_8^{2-} + Fe^0_{(s)} \rightarrow 2SO_4^{2-} + Fe^{2+}_{(aq)} \qquad 1.2\times10^{-1}\ M^{-1}\ s^{-1} \qquad (S1)^2$$

$$S_2O_8^{2-} + Fe^{2+}_{(aq)} \rightarrow SO_4^{\bullet-} + SO_4^{2-} + Fe^{3+}_{(aq)} \qquad 2.0\times10^{1}\ M^{-1}\ s^{-1} \qquad (S2)^3$$

66 $S_2O_8^{2-} + Fe_{(aq)}^{3+} \rightarrow S_2O_8^{\bullet-} + Fe_{(aq)}^{2+}$ 6.6×10^{-2} M^{-1} s^{-1} (S3)[4]

67 The mole fractions of persulfate decomposed by each iron species can be estimated using the
68 branching ratios for reactions S1, S2, and S3,

69

70 $$f_{Si} = \frac{[Fe^n]\times\ k_{Si}}{[Fe^0]\times k_{S1} + [Fe^{2+}]\times k_{S2} + [Fe^{3+}]\times k_{S3}},$$

71

72 where f_{Si} is the mole fraction of persulfate decomposed through reaction S*i*, $[Fe^n]$ is the
73 concentration of Fe species, and k_{Si} is the second-order rate constant for the reaction of interest.

74 The sulfate radical can react with $Fe^{2+}_{(aq)}$ and then be scavenged (reaction S4). Phenol
75 (C_6H_5OH) is oxidized by the sulfate radical (reactions S4 and S5). Reactions S4 and S5 are
76 competitive because the concentrations of the reactants and the reaction rate constants are not
77 markedly different. A sulfate radical can also react with another sulfate radical or with
78 persulfate (reactions S6 and S7). The formation of $SO_4^{\bullet-}$ (reaction S2) is the rate-limiting step
79 for reactions S2, S4, and S5, and any $SO_4^{\bullet-}$ formed will instantly be transformed through
80 reactions S4 and S5. Reaction S6 will therefore make a negligible contribution because of the
81 low steady-state $SO_4^{\bullet-}$ concentration.

82

83 $SO_4^{\bullet-} + Fe_{(aq)}^{2+} \rightarrow SO_4^{2-} + Fe_{(aq)}^{3+}$ 4.6×10^{9} M^{-1} s^{-1} (S4)[3]

84 $SO_4^{\bullet-} + C_6H_5OH \rightarrow SO_4^{2-} + (Byproducts)$ 3.0×10^{9} M^{-1} s^{-1} (S5)[5]

$SO_4^{\bullet-} + SO_4^{\bullet-} \rightarrow S_2O_8^{2-}$ $8.1\times10^8\ M^{-1}\ s^{-1}$ (S6)[5]

$SO_4^{\bullet-} + S_2O_8^{2-} \rightarrow S_2O_8^{\bullet-} + SO_4^{2-}$ $6.3\times10^5\ M^{-1}\ s^{-1}$ (S7)[5]

The persulfate radical can be transformed through reactions S8 and S9. Reaction S9, in which $Fe^{3+}_{(aq)}$ is reduced to $Fe^{2+}_{(aq)}$, can be neglected because the tests we conducted were under acidic conditions. Most of the persulfate radicals will be scavenged through reaction S8, through which sulfate radicals are not formed.

$S_2O_8^{\bullet-} + \frac{3}{2}H_2O \rightarrow 2SO_4^{2-} + \frac{3}{4}O_2 + 3H^+$ (S8)[5]

$S_2O_8^{\bullet-} + Fe^{3+}_{(aq)} + 2OH^- \rightarrow 2HSO_5^- + Fe^{2+}_{(aq)}$ (S9)[5]

The hydroxyl radical forms through radical propagation reactions (reactions S10 and S11). It has been reported that insignificant amounts of $OH^{\bullet}$ form under acidic conditions.

$SO_4^{\bullet-} + OH^- \rightarrow OH^{\bullet} + SO_4^{2-}$ $7\times10^7\ M^{-1}\ s^{-1}$ (S10)[5]

$SO_4^{\bullet-} + H_2O \rightarrow OH^{\bullet} + H^+$ $660\ s^{-1}$ (S11)[5]

In conclusion, reactions S1−S5 will have been the dominant pathways through which persulfate decomposed and sulfate radicals were used in our study.

Kinetic modeling

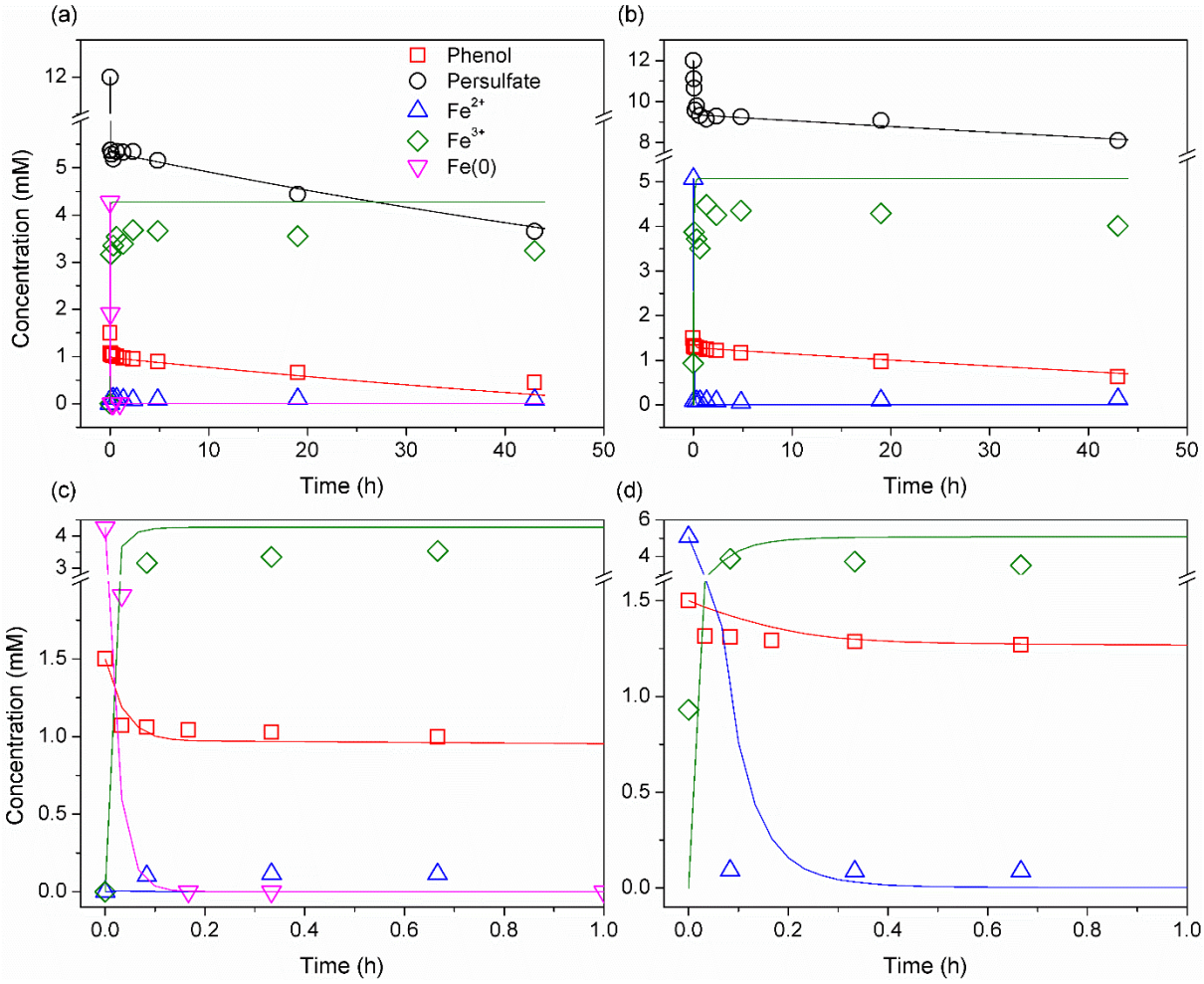

Figure S2. Model fittings of reactions in (a) PS/NZVI and (b) PS/Fe^{2+} systems. Magnified first 1 h fittings are presented in (c) and (d) for both systems, respectively.

111 **Table S1**. Estimated second-order rate constants of reactions

($M^{-1}s^{-1}$)	PS/NZVI	PS/Fe^{2+}
k_{R1}	2.06	
k_{R2}	4.28E+01	4.80E+01
k_{R3}	2.70E-04	9.92E-05
k_{R4}	3.28E+09	8.27E+09
k_{R5}	2.28E+07	9.02E+07

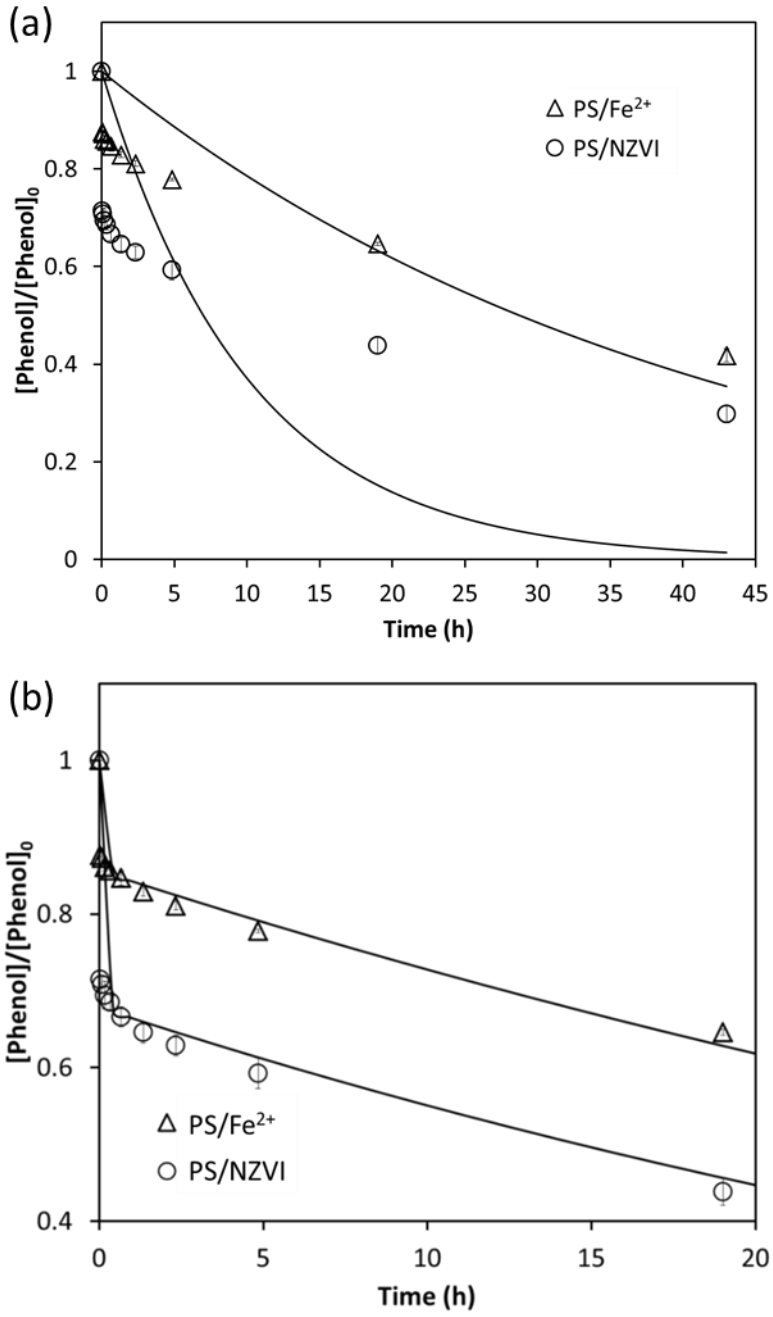

112

113 **Figure S3.** Phenol oxidation kinetic curves fitted using (a) a pseudo-first-order model and (b)
114 a two-compartment first-order model (PS = persulfate, NZVI = nanosized zero-valent iron)

115

Table S2. Parameters for the two-compartment first-order model

	Persulfate/nanosized zero-valent iron	Persulfate/Fe^{2+}
Correlation coefficient (R^2)	0.977	0.998
k_1 (h^{-1})	56.4	32.8
k_2 (h^{-1})	0.020	0.015
Predicted f	0.313	0.143
Observed f (Δ[phenol] after 10 min)	0.306	0.139

Transformation of NZVI in the persulfate/NZVI system

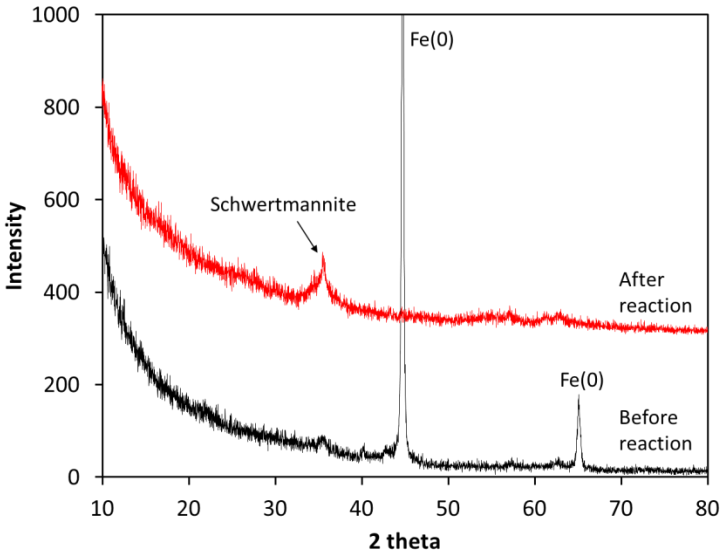

Figure S4. X-ray diffraction patterns for the nanosized zero-valent iron before and after the oxidation process

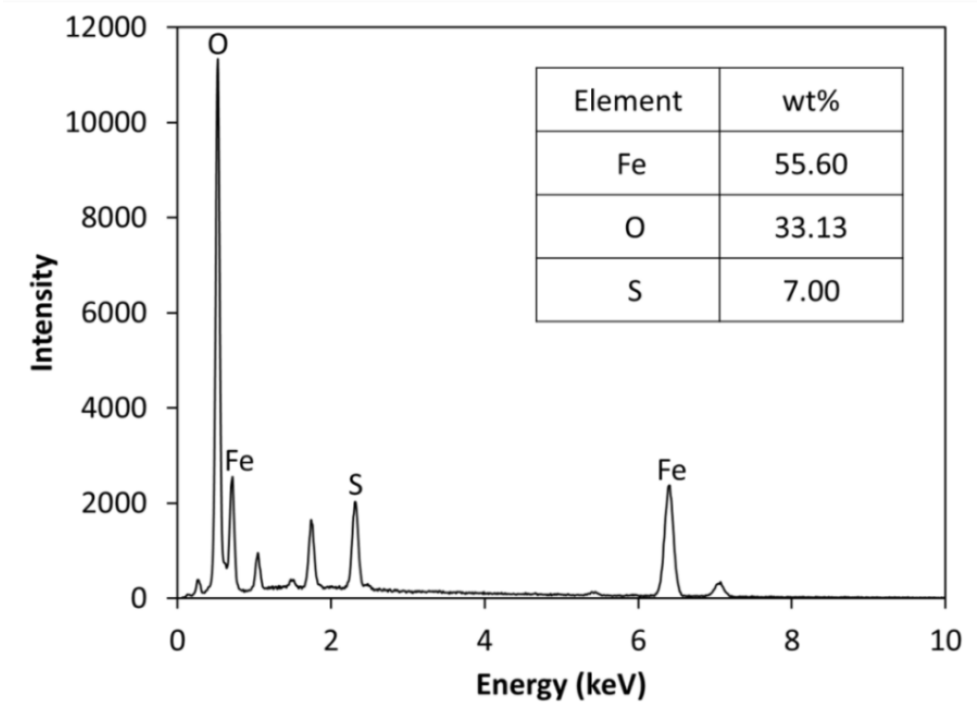

123

124 **Figure S5.** Scanning electron microscopy energy dispersive spectroscopy spectrum for the
125 nanosized zero-valent iron surface after the oxidation process. The inset table shows the
126 elemental composition.

127

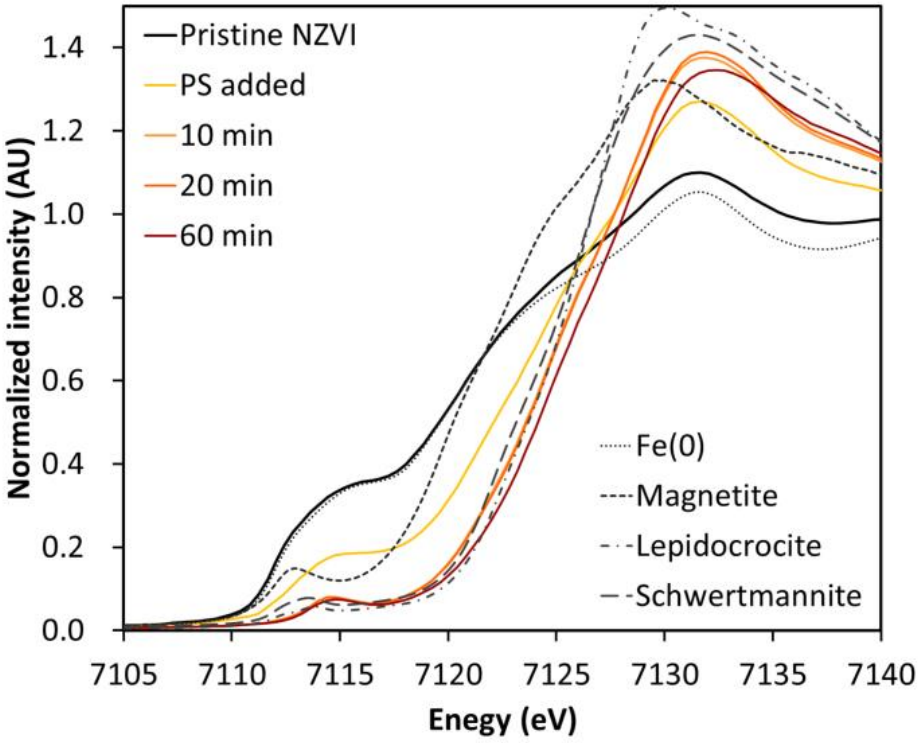

Figure S6. Normalized X-ray absorption near edge structure spectra of the nanosized zero-valent iron (NZVI) particles during the oxidation tests. "PS added" indicates the spectrum of a NZVI sample collected immediately after persulfate had been added to the system. X-ray absorption near edge structure spectra of the four standard iron samples are shown as gray dashed lines. An absorption edge at a higher energy level indicated the NZVI particles were in a higher oxidation state. The spectra for samples collected after 10 and 20 min of the reaction almost overlapped.

Table S3. Quantitative iron speciation results calculated from the linear combination fittings of the X-ray absorption fine structure spectra. The values in parentheses are the uncertainties.

	Pristine	Just after persulfate was added	After 10 min	After 20 min	After 60 min
Fe(0)	71.2 (3.2)	31.3 (0.8)	0.0 (5.3)	0.0 (0.0)	0.0 (0.0)
Magnetite	25.8 (2.1)	50.9 (3.8)	74.4 (0.0)	65.8 (2.2)	51.5 (2.6)
Lepidocrocite	3.0 (2.3)	12.0 (2.9)	12.8 (1.1)	8.3 (3.3)	1.6 (5.2)
Schwertmannite	0.0 (0.0)	5.8 (11.0)	12.8 (0.8)	25.9 (2.5)	47.0 (2.9)

Table S4. Fractions of iron of different valences in the persulfate (PS)/nanosized zero-valent iron (NZVI) and PS/Fe^{2+} systems. $Fe^{2+}_{(s)}$ is one-third of the magnetite molar content. $Fe^{2+}_{(s)}$ is the sum of the lepidocrocite and schwertmannite molar contents plus two-thirds of the magnetite molar content.

Iron species (mM) \ Reaction time (min)		0	10	20
PS/NZVI	$Fe^{0}_{(s)}$	4.27	0	0
	$Fe^{2+}_{(s)}$	0.52	0.63	0.51
	$Fe^{3+}_{(s)}$	1.21	1.90	1.83
	$Fe^{2+}_{(aq)}$	0	0.11	0.11
	$Fe^{3+}_{(aq)}$	0	3.35	3.54
PS/Fe^{2+}	$Fe^{0}_{(s)}$	0	0	0
	$Fe^{2+}_{(s)}$	0	0	0
	$Fe^{3+}_{(s)}$	0	2.19	2.41
	$Fe^{2+}_{(aq)}$	5.07	0.09	0.09
	$Fe^{3+}_{(aq)}$	0.93	3.72	3.50

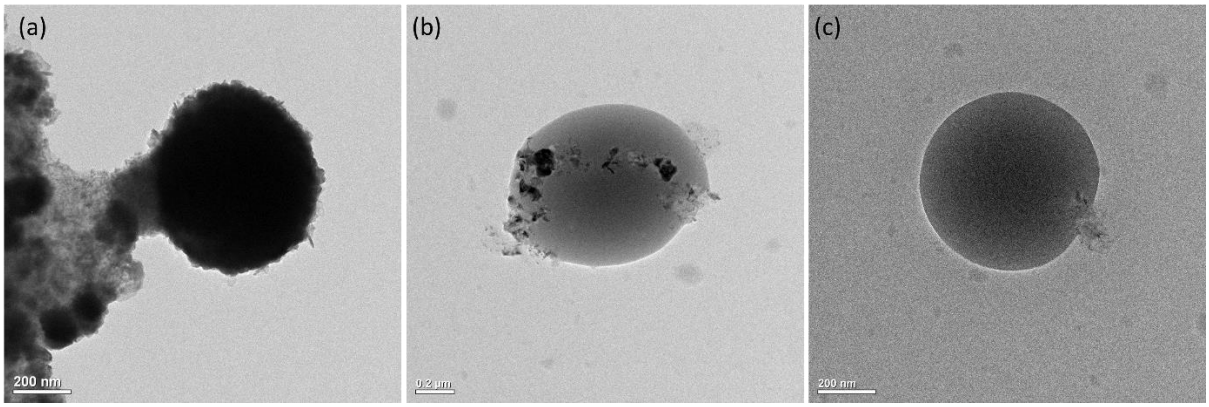

Figure S7. TEM images of (a) pristine NZVI, (b) NZVI just after persulfate was added, and (c) after 1 h in persulfate/NZVI system. Black $Fe^0_{(s)}$ core was substantially consumed and shrank just after persulfate added. After 1 h, no $Fe^0_{(s)}$ was observed.

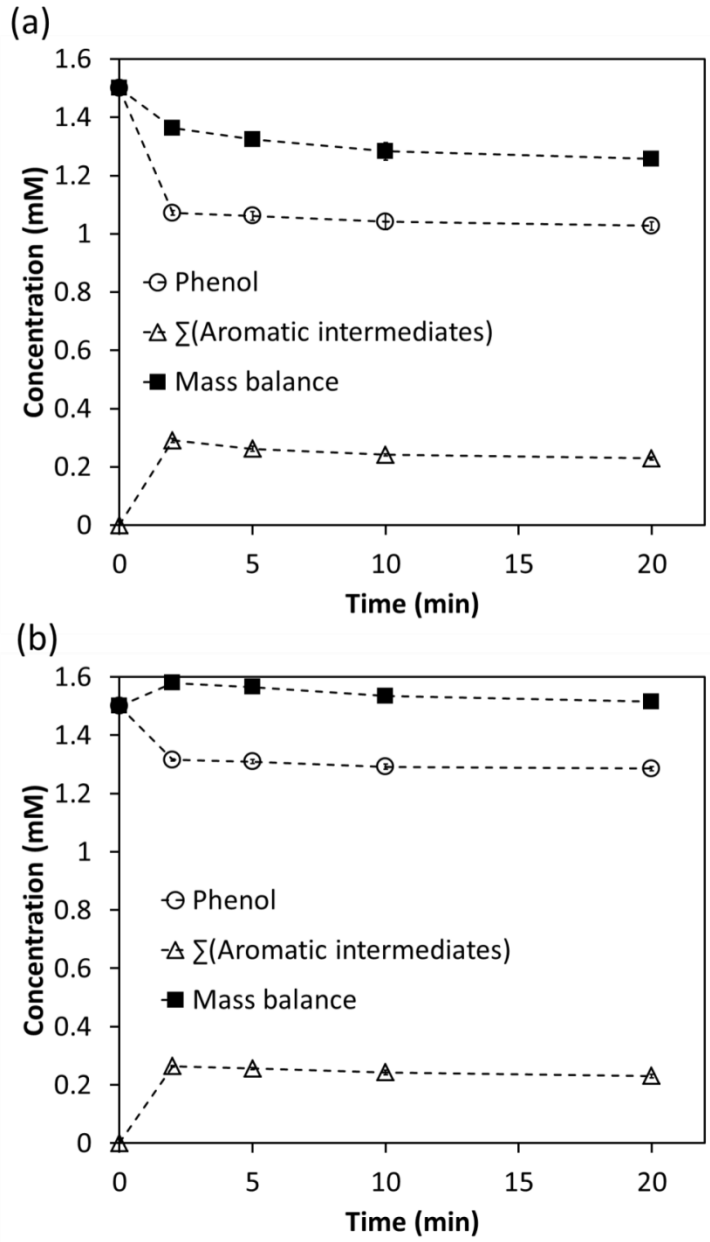

151

152 **Figure S8.** Degradation of phenol and its aromatic intermediates in (a) the persulfate/nanosized
153 zero-valent iron system and (b) the persulfate/Fe^{2+} system

154

Persulfate activation by the NZVI transformation products

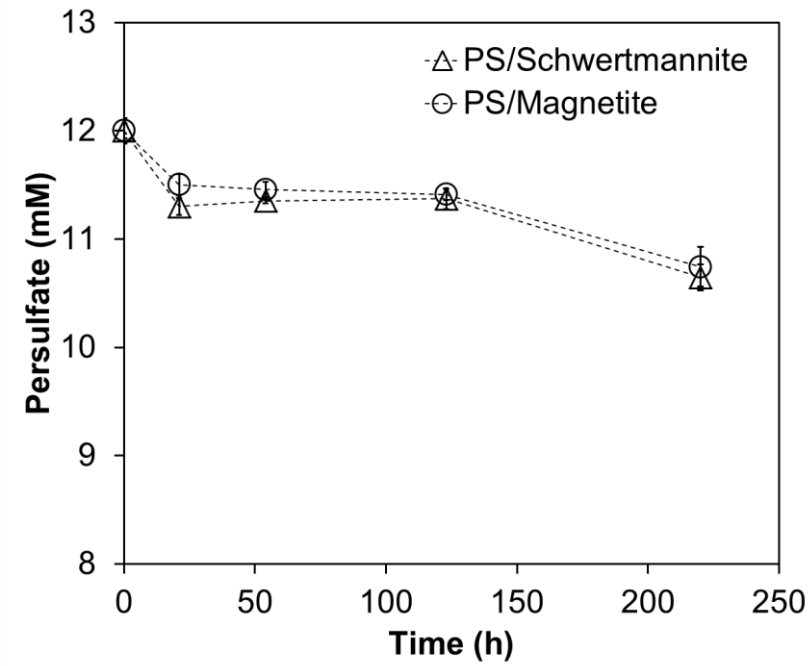

Figure S9. Persulfate consumption in the persulfate (PS)/schwertmannite and PS/magnetite systems. The error bars represent the standard errors for triplicate tests.

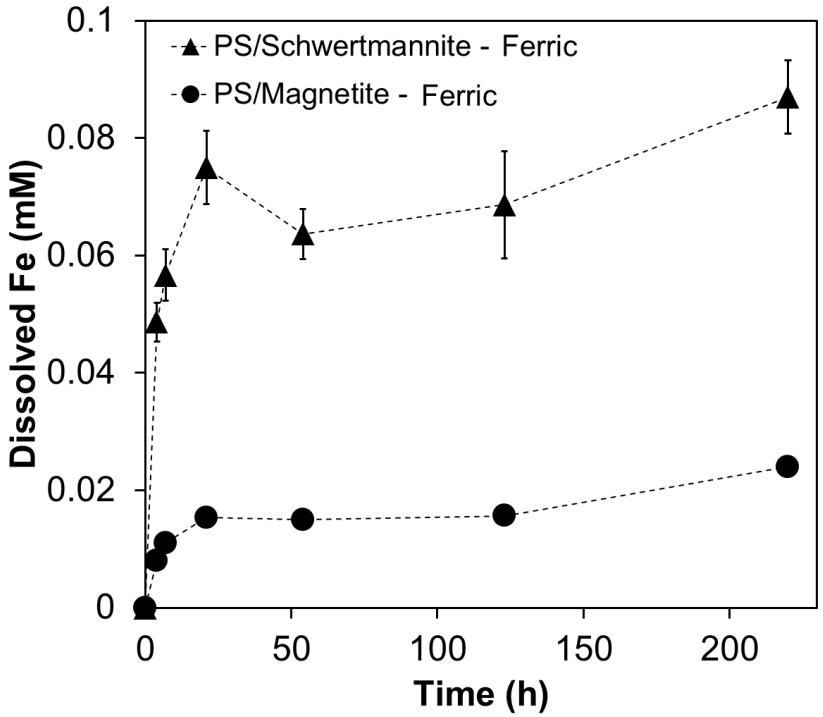

161

162 **Figure S10.** Evolution of dissolved iron in the persulfate (PS)/schwertmannite and
163 PS/magnetite systems. The Fe^{2+} concentrations were negligible in both systems. The error bars
164 represent the standard errors for triplicate tests.

165

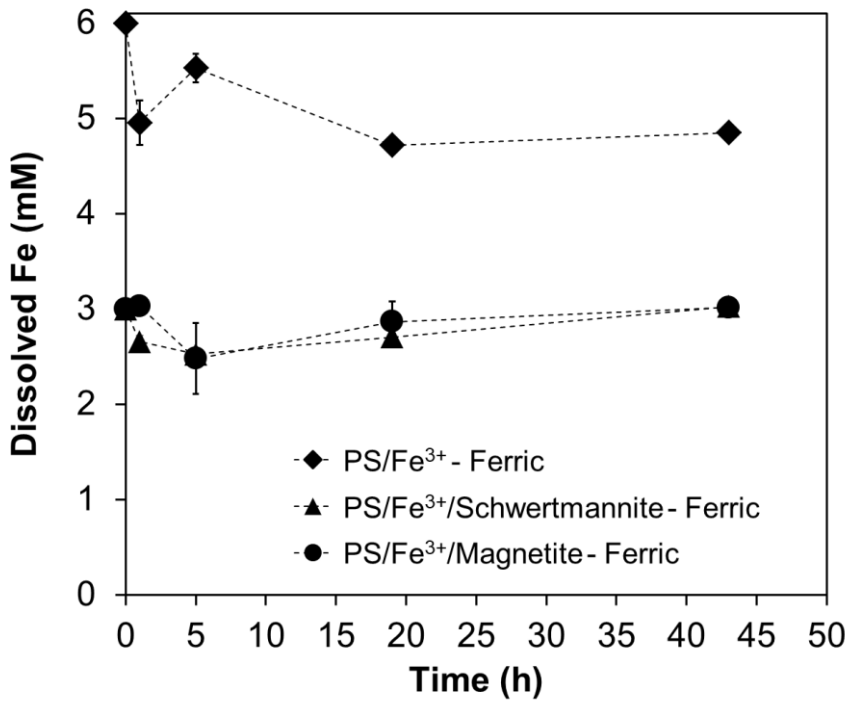

166

167 **Figure S11.** Evolution of dissolved iron in the persulfate (PS)/Fe^{3+}, PS/Fe^{3+}/schwertmannite,
168 and PS/Fe^{3+}/magnetite systems. The Fe^{2+} concentrations were negligible in all three systems.
169 The error bars represent the standard errors for triplicate tests.

170

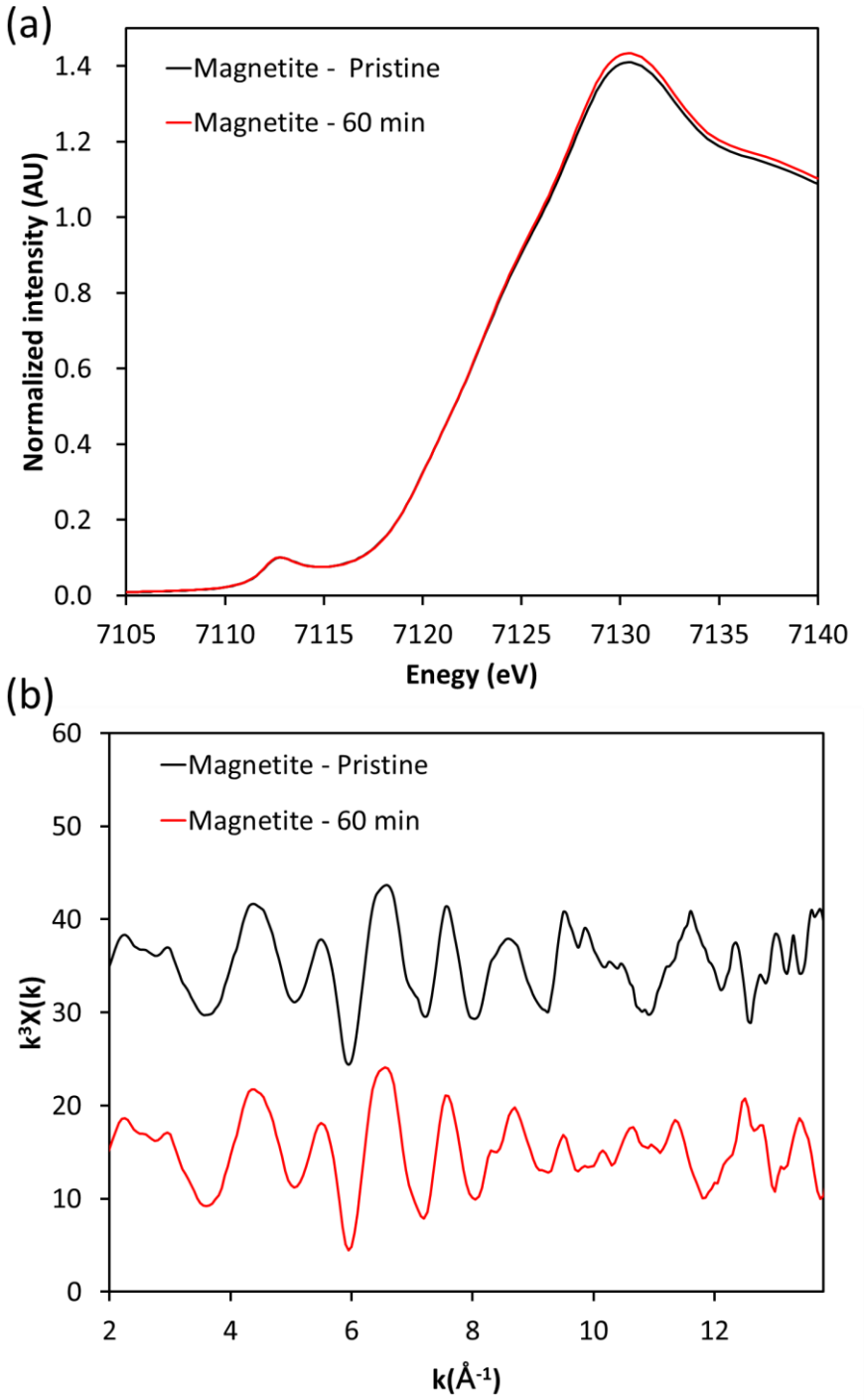

171

172 **Figure S12.** Transformations of magnetite in the persulfate/magnetite system determined from
173 (a) the X-ray absorption near edge structure spectra and (b) the k^3-weighted X-ray absorption
174 fine structure spectra

175

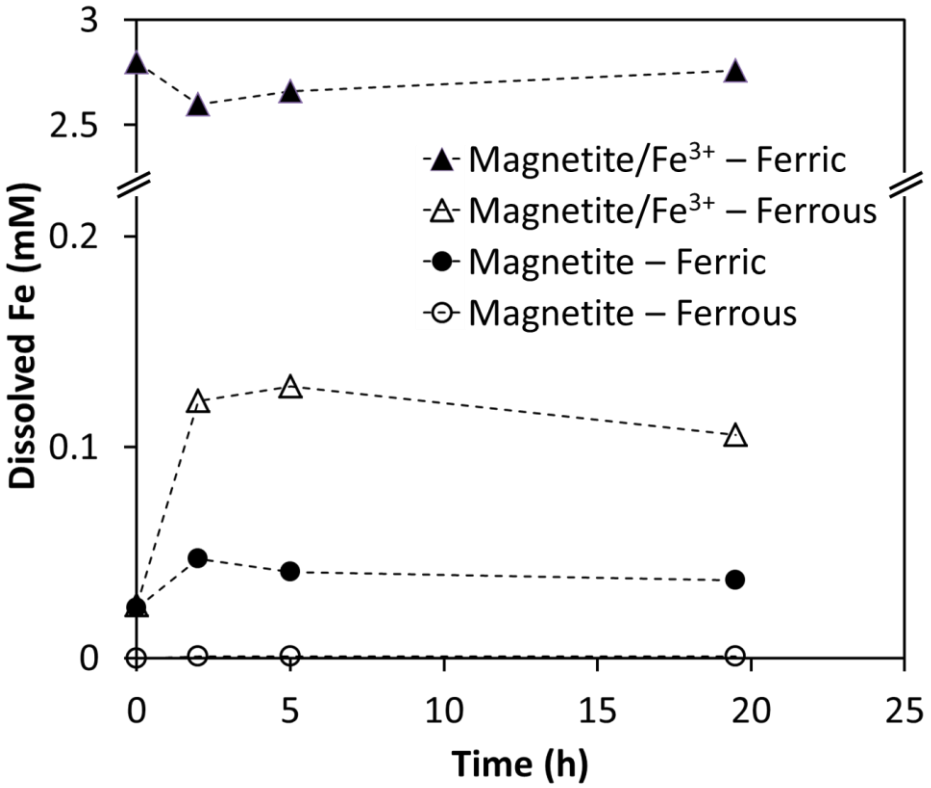

Figure S13. Evolution of dissolved iron in the presence of magnetite/Fe^{3+} and only magnetite

References

(1) Fang, G., Gao, J., Dionysiou, D. D., Liu, C., & Zhou, D. (2013). Activation of persulfate by quinones: free radical reactions and implication for the degradation of PCBs. *Environmental science & technology*, *47*(9), 4605-4611.

(2) Kusic, H., Peternel, I., Ukic, S., Koprivanac, N., Bolanca, T., Papic, S., & Bozic, A. L. (2011). Modeling of iron activated persulfate oxidation treating reactive azo dye in water matrix. *Chemical engineering journal*, *172*(1), 109-121.

(3) Liang, C., & Guo, Y. Y. (2010). Mass transfer and chemical oxidation of naphthalene particles with zerovalent iron activated persulfate. *Environmental science & technology*, *44*(21), 8203-8208.

(4) Li, W., Orozco, R., Camargos, N., & Liu, H. (2017). Mechanisms on the Impacts of

Alkalinity, pH, and Chloride on Persulfate-Based Groundwater Remediation. *Environmental Science & Technology*, *51*(7), 3948-3959.

(5) Liu, H., Bruton, T. A., Li, W., Buren, J. V., Prasse, C., Doyle, F. M., & Sedlak, D. L. (2016). Oxidation of benzene by persulfate in the presence of Fe (III)-and Mn (IV)-containing oxides: stoichiometric efficiency and transformation products. *Environmental science & technology*, *50*(2), 890-898.